High-throughput single-microparticle imaging flow analyzer

Keisuke Goda[a,b,c,1], Ali Ayazi[a], Daniel R. Gossett[b,c], Jagannath Sadasivam[a], Cejo K. Lonappan[a], Elodie Sollier[b,c], Ali M. Fard[a,b], Soojung Claire Hur[b,d], Jost Adam[a], Coleman Murray[c], Chao Wang[a], Nora Brackbill[a], Dino Di Carlo[b,c], and Bahram Jalali[a,b,c,e,f]

[a]Department of Electrical Engineering, University of California, Los Angeles, CA 90095; [b]California NanoSystems Institute, Los Angeles, CA 90095; [c]Department of Bioengineering, University of California, Los Angeles, CA 90095; [d]Department of Mechanical and Aerospace Engineering, University of California, Los Angeles, CA 90095; [e]Department of Surgery, David Geffen School of Medicine, University of California, Los Angeles, CA 90095; and [f]Eli and Edythe Broad Center of Regenerative Medicine and Stem Cell Research, David Geffen School of Medicine, University of California, Los Angeles, CA 90095

Edited by David A. Weitz, Harvard University, Cambridge, MA, and approved June 6, 2012 (received for review March 22, 2012)

Optical microscopy is one of the most widely used diagnostic methods in scientific, industrial, and biomedical applications. However, while useful for detailed examination of a small number (<10,000) of microscopic entities, conventional optical microscopy is incapable of statistically relevant screening of large populations (>100,000,000) with high precision due to its low throughput and limited digital memory size. We present an automated flow-through single-particle optical microscope that overcomes this limitation by performing sensitive blur-free image acquisition and nonstop real-time image-recording and classification of microparticles during high-speed flow. This is made possible by integrating ultrafast optical imaging technology, self-focusing microfluidic technology, optoelectronic communication technology, and information technology. To show the system's utility, we demonstrate high-throughput image-based screening of budding yeast and rare breast cancer cells in blood with an unprecedented throughput of 100,000 particles/s and a record false positive rate of one in a million.

photonics | microfluidics | instrumentation | high-throughput screening | medical diagnostics

Optical microscopy is one of the most widely used methods in a diverse range of advanced research, industrial, and clinical settings, including microelectronics, food science, oceanography, archaeology, environmental science, energy science, microbiology, mineralogy, and pathology (1–3). High information content spatial metrics provided by imaging are used to characterize microscopic particles such as emulsions, microorganisms, and cells in particle synthesis, ecosystem monitoring, biofuel formulation, drug discovery, histopathology, and cytology-based diagnostics (3–5). An impressive arsenal of optical nanoscopy methods enables imaging of cellular structures beyond the diffraction limit of light (6–8). Unfortunately, while there has been breathtaking progress in improving spatial resolution in the last two decades, mostly overlooked is the temporal resolution of imaging systems.

While useful for visual inspection of many individual microparticles without human intervention, conventional automated microscopy does not have high throughput and is hence unable to evaluate, analyze, and screen large populations with high statistical accuracy. High-throughput detection is essential to rapidly assay morphological and biochemical properties in a reasonable period of time. Unfortunately, the throughput of state-of-the-art automated microscopes is only up to approximately 1,000 particles/s (9–12), limiting the particle count. As a benchmark, this throughput is significantly lower than that of single-pixel high-throughput flow analyzers such as electronic particle counters (13, 14) and flow cytometers (approximately 100,000 particles/s) (15, 16), which trade increased throughput for a lack of spatial resolution. Because of this trade off, such systems are often unable to resolve single, multiple, and clustered particles or unusually shaped particles as well as to distinguish debris and nonspecific labeling and hence produce a large number of false positive events or inaccurate subpopulation counts.

While high-end digital cameras [i.e., charge-coupled device (CCD) and complementary metal-oxide-semiconductor (CMOS) cameras] are now able to perform imaging at a speed approaching 1 million frames/s (17–19), they are not well suited for high-throughput microscopy. First, a critical limitation that hampers imaging of particles flowing at high speeds is the relatively long shutter speed or exposure time (≥1 μs) (17–19) that results in motion blur and loss of resolution during the high-speed flow, hence degrading specificity. Another limitation is the time needed to download the image from the array of thousands of pixels. To achieve high frame rates, the number of pixels that are employed must be reduced in a process known as partial readout (17–21). The penalty is that image resolution is lost at high frame rates. Furthermore, there is a fundamental trade off between sensitivity and speed—at high frame rates, fewer photons are captured during each frame, leading to reduction in sensitivity. Finally, currently digital image processing cannot be performed in real time due to the storage and access of the massive amount of digital data that is produced during high-speed imaging and hence requires many days of off-line digital processing. This translates into a limited particle count, thus compromising statistical precision in high-throughput screening. These limitations prevent automated microscopy from analyzing a large population of particles with high statistical precision in a practical period of time.

To address the needs and fill in the technological gap between the automated microscope and high-throughput flow analyzer, we propose and demonstrate an automated flow-through single-particle optical microscopy system that can evaluate, analyze, and screen a large population of particles with high specificity, high sensitivity, and high statistical precision in a short time. This method builds on a unique integration of (*i*) an ultrafast optical imaging modality known as serial time-encoded amplified microscopy (STEAM) (22, 23) for blur-free imaging of particles in high-speed flow, (*ii*) inertial microfluidic technology for sheath-free focusing and ordering of particles with inertial forces (24, 25), and (*iii*) hybrid optoelectronic image processing circuitry for

Author contributions: K.G. designed research; K.G., A.A., D.R.G., J.S., C.K.L., E.S., C.W., and N.B. performed research; K.G., D.R.G., J.S., C.K.L., E.S., A.M.F., S.C.H., and C.M. contributed new reagents/analytic tools; K.G., A.A., J.S., C.K.L., A.M.F., J.A., and C.W. analyzed data; and K.G., A.A., D.R.G., D.D.C., and B.J. wrote the paper.

The authors declare no conflict of interest.

This article is a PNAS Direct Submission.

Freely available online through the PNAS open access option.

[1]To whom correspondence should be addressed. E-mail: goda@ee.ucla.edu.

This article contains supporting information online at www.pnas.org/lookup/suppl/doi:10.1073/pnas.1204718109/-/DCSupplemental.

real-time image processing. The integrated system transforms particles in well-controlled microfluidic flow into a series of E-slides—an electronic version of glass slides—on which particles of interest are digitally analyzed. With the power of optoelectronic communication and information technologies, this property enables fully automated real-time image-recording and classification of a large number of particles through their morphological and biochemical features. To demonstrate our technology's utility, we show real-time nonstop image-based identification and screening of budding yeast cells at different budding stages and rare breast cancer cells in blood with an unprecedented throughput of 100,000 particles/s and a record false positive rate of one in a million.

Results

Principle of the High-Throughput Imaging Flow Analyzer. Our system, which we refer to as the STEAM flow analyzer (Fig. 1*A* and *SI Text* and Table S1), consists of three subsystems: (*i*) the microfluidic device (Fig. 1*B* and *SI Text* and Table S2), (*ii*) the STEAM camera (Fig. 1*A* and *SI Text* and Table S1), and (*iii*) the real-time optoelectronic time-stretch image processor (Fig. 1*C* and *SI Text* and Table S3). An animated video (Movie S1) shows the integrated functionality of the system. The STEAM flow analyzer operates in three steps. First, particles are controlled to flow at a uniform velocity and focused and ordered by inertial lift forces in the microfluidic channel. Second, the STEAM camera takes images of the fast-flowing particles. Finally, the real-time optoelectronic time-stretch image processor processes the images optically and electronically and then performs automated particle screening in real time.

The STEAM flow analyzer employs inertial microfluidic technology (Fig. 1*B* and Movie S1). This method provides uniform positions and velocities for particles through intrinsic inertial lift forces (important for generation of clear E-slides) while eliminating the need for sheath fluid, which is traditionally required for hydrodynamic focusing in conventional flow cytometers. While inertial forces are typically assumed to be negligible in microfluidic systems, they can, in fact, be important when the flow rate in microchannels is high. Particles in finite-inertia confined channel flows focus to cross-sectional dynamic equilibrium positions that correspond with the fold of symmetry of the channel cross-section (26). Furthermore, longitudinal ordering (i.e., stabilizaed interparticle or intercell spacing along the length of the channel) results from inertial lift forces and the flow field acting together (27). In some of our previous work, we determined an optimal balance between inertial lift forces and Dean drag forces, counter-rotating vortices perpendicular to primary channel flow, to accurately position a range of particle sizes to a single streak with two heights within the channel at a high flow rate (26). Here we reduced the length of one of these optimized channels to decrease its pressure and lowered the height of the channel to bring the distinct equilibrium positions in the vertical plane into closer proximity. To ensure stability in real-time image processing, the microfluidic device was fabricated by replica molding in thermoset polyester due to its high stiffness and ability to sustain high pressures (*SI Text*, Fig. S1, and Table S2) (28).

The STEAM camera first captures fast sequential images with laser pulses and then stretches image-encoded pulses in time so that they can be digitized and processed in real time (see *SI Text*). During the time-stretch process, images are also optically amplified to overcome the thermal noise inherent in photon-to-electron conversion. In the first step, a pair of diffraction gratings spatially disperses the broadband optical pulse into a rainbow designed to capture 1D line scans of particles flowing through the channel. The temporal duration of these pulses is 27 ps (shutter speed), and they occur at a repetition rate of 36.7 MHz (line scan rate), while the average illumination power is 500 μW. The back-reflected pulses from the microfluidic device are directed via

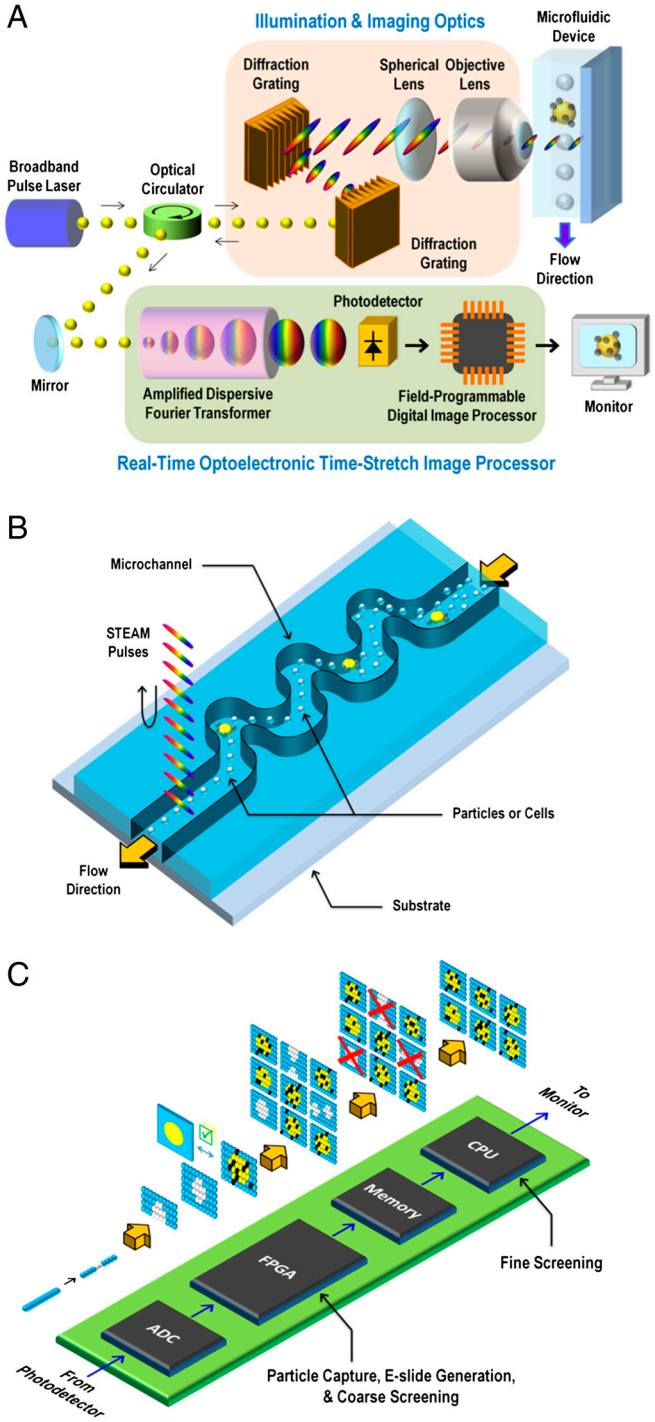

Fig. 1. STEAM flow analyzer. An animated video that shows the integrated functionality of the system is available (Movie S1). (*A*) Schematic of the STEAM flow analyzer that highlights the optical layout of the STEAM camera and real-time optoelectronic time-stretch image processor. The STEAM camera takes blur-free images of fast-flowing particles in the microfluidic device. The acquired images are optoelectronically processed and screened in the real-time optoelectronic time-stretch image processor. (*B*) Microfluidic device in which particles are controlled to flow at a uniform velocity and focused and ordered by inertial lift forces in the microfluidic channel. (*C*) Field-programmable digital image processor that captures particles and performs fully automated particle classification in real time. It consists of (*i*) a high-speed analog-to-digital converter (ADC); (*ii*) a field-programmable gate array (FPGA) for particle capture, E-slide generation, and coarse particle classification; (*iii*) an on-board memory circuit for storing selected E-slides; and (*iv*) a central processing unit (CPU) for fine particle classification.

an optical circulator toward the real-time optoelectronic time-stretch image processor followed by the high-speed photodetector and the field-programmable digital image processor. Two-dimensional E-slides are then constructed from the digitized 1D frames and made available for screening.

As shown in Fig. 1*A*, the real-time optoelectronic time-stretch image processor consists of an amplified dispersive Fourier transformer (29–32), a high-speed photodetector, and a field-programmable digital image processor. First, the amplified dispersive Fourier transformer serializes the image-encoded pulse (i.e., the 1D image frame) into a pixel stream that is slowed down in time so that it can be digitized and processed in real time. While it is being stretched in time, the image-carrying pulse is amplified in the optical domain through distributed Raman amplification in the time-stretch element. Raman amplification is chosen because it has a broad and flexible optical spectrum and also leads to low noise figure in the frequency-to-time mapping process (29–32). The optical image amplification (approximately 1,000x) before photon-to-electron conversion is critical as it enables high-throughput microscopy in the ultrashort exposure time (27 ps) without the need for a high-intensity illuminator. In addition, the ultrafast shutter speed freezes any motion of particles in high-speed flow, allowing for acquisition of blur-free images. The amplified 1D data stream is detected by the high-speed single-pixel photodetector, eliminating the need for a detector array and hence readout time limitations. After analog-to-digital conversion by a real-time digitizer, the data is processed in real time in the field-programmable digital image processor with a programmable multi-stage decision-making architecture (Fig. 1*C* and Movie S1 and *SI Text*) that employs a field-programmable gate array (FPGA) (33, 34), an on-board memory circuit, and a central processing unit (CPU). Specifically, the function of the FPGA is to identify the presence of particles (ignoring the unimportant space between the particles), generate E-slides for the particles, coarsely down-select the slides (i.e., the particles) through their morphological and biochemical markers, and store those selected in the memory. As a second-step screening process, the CPU performs fine particle classification on the stored slides with more stringent algorithms such as decision-tree classification and supervised learning methods (35, 36).

The STEAM flow analyzer's blur-free image acquisition enables differentiation of particles from a heterogeneous population. Fig. 2 shows E-slides of fast-flowing particles of various species in the microfluidic channel captured by the STEAM flow analyzer. Here the particles were controlled to flow at a uniform speed of 4 m/s, which corresponds to a throughput of 100,000 particles/s—a very fast flow, but motion blur is absent in the images due to the ultrafast shutter speed of the STEAM camera (27 ps). For comparison, Fig. 2 also shows images of the same types of particles under the same flow conditions captured by a state-of-the-art CMOS camera (see *SI Text*). These images show that the CMOS camera's lower shutter speed (1 μs) and lack of optical image amplification significantly reduced the sensitivity and caused motion blur in the images, rendering the camera unable to classify particles reliably. For further comparison, stationary particles of the same types on a glass slide were obtained under a conventional microscope with a CCD camera with a much longer exposure time (shutter speed) of 17 ms (Fig. 2 and Fig. S2). Despite the fact that the STEAM camera is many orders of magnitude faster than the CCD camera, the two cameras share similar image quality (i.e., sensitivity and resolution).

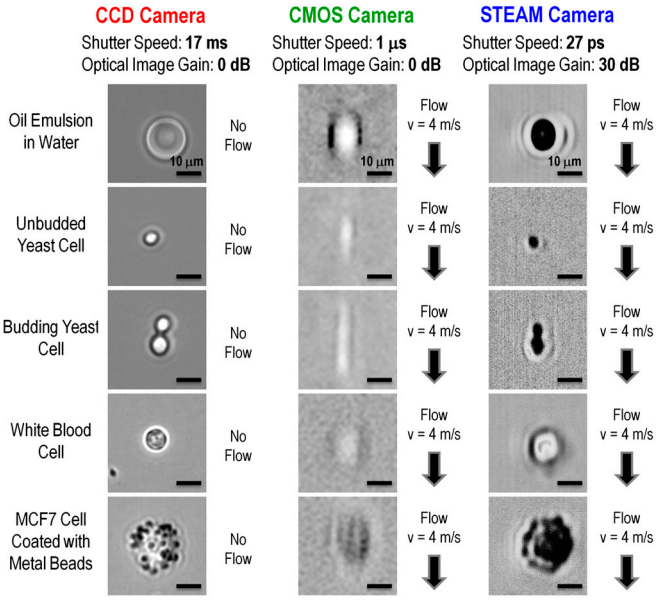

Fig. 2. Performance of the STEAM camera and comparison with a conventional CCD camera and a state-of-the-art CMOS camera. E-slides of flowing particles of various species in the microfluidic device were generated by the STEAM flow analyzer with the built-in STEAM camera (27 ps shutter speed, 128 × 512 pixels, 25 dB optical image gain). The E-slides are compared with images of the same particles captured by a state-of-the-art CMOS camera (1 μs shutter speed, 32 × 32 pixels, no optical image gain) under the same flow. To operate at these high speeds, the CMOS camera used partial readout, limiting the number of pixels to 32 × 32. Here the particles were controlled to flow at a uniform speed of 4 m/s, which corresponds to a throughput of 100,000 particles/s based on the volumetric flow rate. The high-speed motion of the particles was frozen by the ultrafast shutter speed (ultrashort exposure time) of the STEAM camera (27 ps) yet without sacrificing sensitivity due to the optical image amplification whereas the reduced sensitivity and motion blurs caused by the CMOS camera's much lower shutter speed and lack of optical image amplification are evident. For further comparison, stationary particles of the same types on a glass slide were obtained under a conventional microscope with a CCD camera with a much longer exposure time (17 ms shutter speed, 1,280 × 1,024 pixels, no optical image gain). Despite the fact that the STEAM camera is many orders of magnitude faster than the CCD camera, the two cameras share similar image quality (i.e., sensitivity and resolution).

Screening of Budding Yeast with the High-Throughput Imaging Flow Analyzer. To show the utility of the STEAM flow analyzer, we used it to demonstrate high-throughput screening of *Saccharomyces cerevisiae*, commonly known as budding yeast. Budding yeast are important in food science, are used as a model for studying eukaryotic cell biology, and are engineered to produce protein therapeutics. Growth in yeast can be studied and optimized by flow cytometry or microscopy—both of which possess specific limitations. Biochemical analysis alone via flow cytometry is insufficient for analysis of complex checkpoints and detection of minor perturbations in the cell cycle (37) and provides poor characterization of the asymmetric growth of yeast in comparison with imaging (38). A high-throughput microscopy technique such as our STEAM flow analyzer could provide a powerful screening tool to assay morphological changes potentially accompanying systematic gene knockouts or other molecular perturbations.

The STEAM flow analyzer can efficiently identify and screen budding yeast cells and perform subpopulation analysis in real time. Here we programmed the FPGA and CPU to capture incoming cells, distinguish between budding and unbudded cells, and classify budding cells based on different budding stage (Fig. 3*A* and *SI Text*). Specifically, the FPGA performs cell capture while ignoring the blank images and stores the corresponding E-slides in the on-board memory (1 GB) which can save up to approximately 16,000 v slides (each of which has 64/v KB), where v is the flow speed in units of m/s (Fig. S3*A*). Here because the 2D E-slides are constructed from a series of 1D frames with the second dimension provided by the flow, the size of each slide decreases, and hence the total number of slides that can be saved in the memory increases as the flow speed increases. We estimate

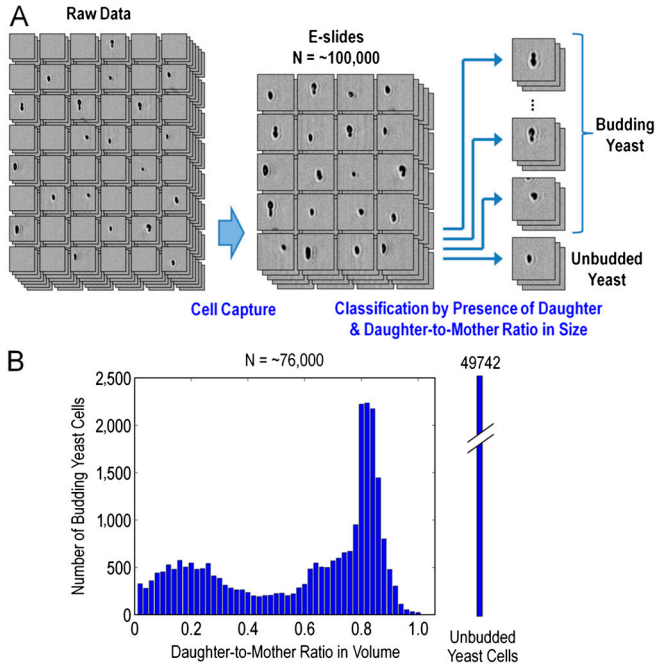

Fig. 3. High-throughput screening of budding yeast with the STEAM flow analyzer. (*A*) Screening process of the field-programmable digital image processor. The FPGA performs cell capture while ignoring the blank images between cells and stores the corresponding E-slides into the on-board memory. The CPU then distinguishes between budding and unbudded cells, classifies the budding cells by daughter-to-mother ratio in size, and finally generates a histogram for the subpopulations. (*B*) Subpopulation analysis of yeast at different stages of budding. The total number of captured yeast cells is 75,509, about 34% of which constitutes budding cells. Here the entire procedure that consists of the measurement, image analysis, and histogram generation takes less than a few minutes. Because the STEAM flow analyzer operates in real time, time-resolved statistical analysis of the subpopulations can also be performed to control and optimize the budding process. Furthermore, similar capture and subpopulation analysis can also be applied to emulsions for applications in cosmetics and pharmaceutics.

that the flow speed can be set up to 8 m/s (corresponding to 200,000 cells/s) while retaining reasonable image quality and classification precision. The saved E-slides are then subject to the CPU's classification process (Fig. S3*B*) in which the budding yeast cells are isolated and classified by daughter-to-mother ratio in size to generate a histogram for the subpopulations using a decision-tree classification method (Fig. 3*B*). For comparison, we also performed normal microscopic observation of yeast cells with a CCD camera and performed digital image processing similar to the automated classification on the CPU in the STEAM flow analyzer and found good agreement between our high-throughput method and the conventional method (Fig. S3*C*), suggesting that the STEAM flow analyzer is useful for analysis of yeast growth behavior with high statistical precision. Because the STEAM flow analyzer operates in real time, time-resolved statistical analysis of the subpopulations can also be performed to control and optimize the budding process. Furthermore, similar capture and subpopulation analysis with real-time feedback is expected to be useful for optimization of emulsions for applications in cosmetics and pharmaceutics.

Rare Cell Detection with the High-Throughput Imaging Flow Analyzer. To further show the utility of the STEAM flow analyzer, we used it to demonstrate rare cell detection. While statistically insignificant and hence often ignored, rare events among a large heterogeneous population of cells in blood such as hematopoietic stem cells (39), antigen-specific Tcells (40), and circulating tumor cells (41, 42) (Table S4) are important in biomedical research as well as medical diagnostics and therapeutics (43). Such rare cells can be identified by a combination of morphological (i.e., size, circularity, and clustering) and biochemical (i.e., surface antigens) markers. Here our model for rare cells is the MCF7 cell line (breast cancer) spiked in blood. Red blood cells are lysed with a hypotonic lysing agent while MCF7 cells are fixed with formaldehyde and coated with metal beads with a diameter of 1 μm via an antibody to EpCAM (a cell surface molecule that exists on the surface of epithelial cells but not on the surface of blood cells). Our observation under a conventional microscope indicates that approximately 80% of MCF7 cells are coated with 5–20 metal beads (Fig. S2).

To demonstrate how surface marker detection could be achieved and coupled with morphological analysis in our system, we performed off-line statistical analysis of white blood cells and coated MCF7 cells. This validation is important because it is required to build a fully trained model for our supervised learning method or support vector machine (SVM) (35, 36) to be implemented on the FPGA and CPU (see *SI Text*). The SVM model predicts whether a new target (i.e., cell) falls into any of the predefined cell categories and is then used to identify the target cells in real time. Fig. 4*A* shows scatter plots of white blood cells and MCF7 cells based on the cell size (i.e., diameter) and presence of surface antigens (i.e., metal beads) produced by our system. The plots indicate that the system is capable of differentiating most white blood cells and MCF7 cells with high specificity using a single molecular marker. For comparison, Fig. S4*A* shows, using a conventional flow cytometer, scatter plots of the same cell types based on forward- and side-scattered light intensities as well as PerCP/Cy5.5-antiCD45 and FITC-antiEpCAM (fluorescence markers), which selectively bind to white blood cells and MCF7 cells, respectively (see *SI Text*). The scattered light intensity plots do not allow for differentiation of the two cell types due to the significant overlap between the two groups. Furthermore, the overlap in the fluorescence intensity limits the specificity of the instrument down to approximately 0.1% subpopulations—inadequate for identification of a cell type that is rarer than 0.1% of the population (Table S4).

With the fully trained cell classification model, the STEAM flow analyzer can detect MCF7 cells as rare as one in a million in a short period of time. Here we programmed the FPGA and CPU such that the FPGA captures incoming cells and performs size-based cell classification (Fig. S4*B*) while the CPU performs classification by circularity and presence of metal beads (see *SI Text*). The threshold for the size-based selection is set such that smaller MCF7 cells are also selected at the expense of detecting larger white blood cells (Fig. 4*A*). Yet, this process efficiently rejects more than 99.9995% of white blood cells, all residual red blood cells, and all free-floating metal beads, leaving only a small number of false positive events (on the order of 100 per mL of lysed blood) along with true positive events (Fig. 4*B*). The FPGA's ability to filter out the large number of blood cells and avoid storing the massive amount of digital data enables nonstop real-time operation. The down-selected E-slides (i.e., cell images) are stored in the memory (1 GB) which can save up to approximately 4,000 v slides (each of which has 256/v KB), where v is the flow speed in units of m/s as described above. The stored slides are then subject to the CPU's selection process in which the cells are further classified by circularity and presence of metal beads (Fig. S4*C*). This process rejects almost all the false positive events (i.e., multiple, unfocused, or unordered white blood cells) that have survived from the initial selection process on the FPGA while leaving true positive events and a very small number of false positive events (on the order of 10 per mL of lysed blood), which arise due to image processing artifacts and can further be rejected by human visual inspection (Fig. S4*D*).

Our statistical analysis of the capture efficiency indicates that the field-programmable digital image processor can identify

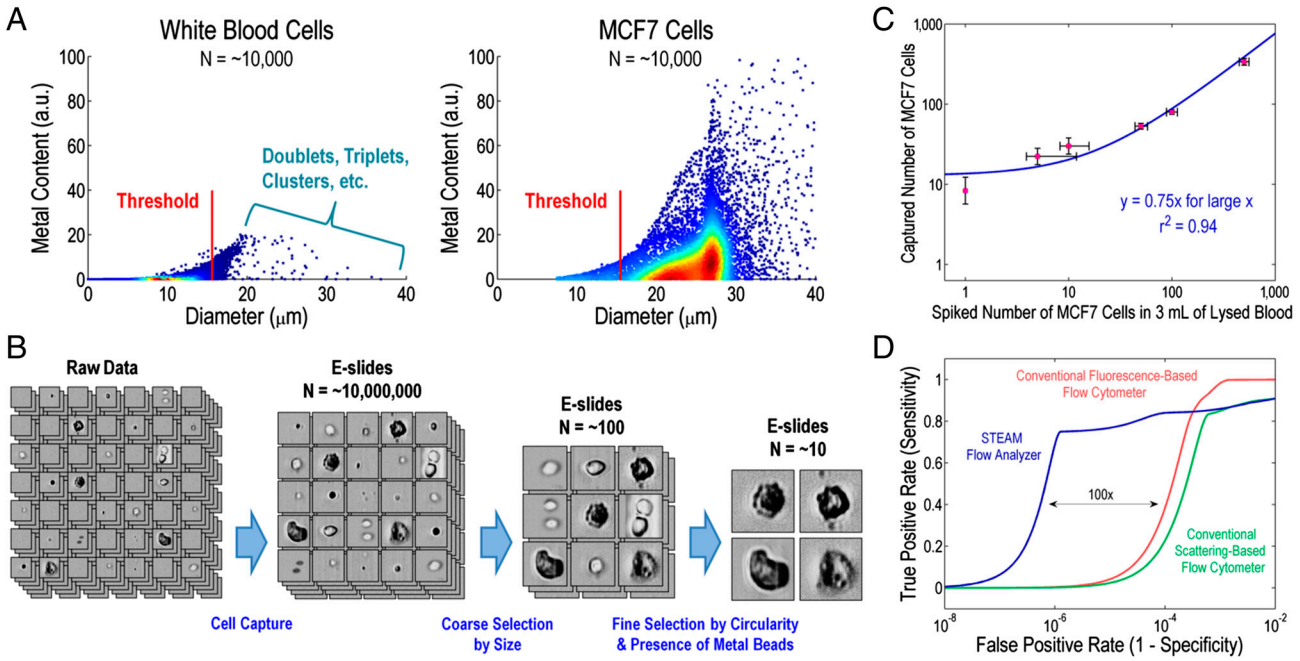

Fig. 4. Rare cell detection with the STEAM flow analyzer. (*A*) Scatter plots of white blood cells and MCF7 cells based on the cell size (i.e., area) and the presence of the surface antigens (i.e., metal beads). The total number of events is approximately 10,000 for both cell types. This statistical analysis is used to build a model and train the supervised learning method and hence the algorithms to run the field-programmable digital image processor. The threshold for the size-based selection performed on the FPGA is set such that smaller MCF7 cells are also selected at the expense of detecting larger white blood cells. The rare white blood cell events that overlap with the distribution of MCF7 cells are doublets or clusters and can hence be rejected by imaging (which is not possible with single-point detection methods). (*B*) Selection process of the field-programmable digital image processor. The FPGA performs cell capture, coarse size-based classification, and filters out more than 99.9995% of white blood cells while leaving only false positive events of the order of 100 per mL of lysed blood along with true positive events. The CPU then performs fine classification by circularity and presence of metal beads and further down-selects cells by an order of magnitude, leaving true positive events and false positive events of the order of 10 per mL of lysed blood, which arise due to image processing artifacts which can further be rejected by human visual inspection. (*C*) Statistical analysis of the system's capture efficiency for various concentrations. The results indicate that the field-programmable digital image processor can identify extremely rare cell with a high efficiency of 75% (limited by the imperfect coating efficiency and missing smaller MCF7 cells in the FPGA selection process). Here all the measurements were performed with bead-coated MCF7 cells spiked in buffer containing white blood cells from 3 mL of lysed blood (approximately 80 million white blood cells) at a throughput of 100,000 cells/s. Individual samples were measured four times, establishing that the classification is highly repeatable (indicated by the vertical error bars). Moreover, the correlation of detected MCF7 cells with spiked MCF7 cells is good ($r^2 = 0.94$). The horizontal deviations can be attributed to several known sources of error in the spiking method including the initial hemacytometer count (see *Materials and Methods*). (*D*) ROC curve analysis of the STEAM flow analyzer in comparison with the conventional flow cytometer. Our method is sufficiently sensitive for detection of approximately one MCF7 cell in a million white blood cells (i.e., a false positive rate of approximately 10^{-6}) and is two orders of magnitude better in terms of false positive rate than the conventional scattering- and fluorescence-based flow cytometer yet without sacrificing throughput.

extremely rare cells with a high efficiency of 75% (limited by the imperfect coating efficiency and missing smaller MCF7 cells in the FPGA selection process) (Fig. 4*C*). Furthermore, our receiver operating characteristic (ROC) (44, 45) curve analysis of the results indicates that our method is sufficiently sensitive for detection of approximately one MCF7 cell in a million white blood cells and is 100 times better in terms of false positive rate than the conventional flow cytometer (Fig. 4*D*) yet without sacrificing throughput (see *SI Text*). Here all the measurements were performed at a throughput of 100,000 cells/s, corresponding to screening of 10 mL of lysed blood in less than 15 min.

Discussion

We have developed a high-throughput single-microparticle flow-through image analyzer for real-time image acquisition and screening of a large heterogeneous population of particles. By overcoming the technological limitations that exist in conventional automated microscopes (with many pixels and a throughput of approximately 1,000 particles/s) (Table S5) and high-throughput flow analyzers (with a single pixel and approximately 100,000 particles/s throughput), our system has achieved real-time image-based screening with high sensitivity (75%), high specificity (one in a million), and high statistical precision (approximately 100,000 particles/s) simultaneously. Here the throughput is only limited by the microfluidic device's tolerance to high pressures caused by high flow rates, not the STEAM camera's image acquisition speed or the field-programmable digital image processor's processing speed. We estimate that the throughput can be increased to 200,000 particles/s while retaining reasonable image quality and classification precision (Table S1). Our method can also be combined with a conventional cell sorter to sort out rare target cells for further genetic analysis of the cells. Furthermore, our method can, in principle, work at shorter wavelengths for higher spatial resolution, provided that proper optical components are available.

While in our proof-of-concept demonstration, we showed high-throughput screening of budding yeast and detection of rare breast cancer cells spiked in blood, our method should also be amenable to other applications in which high-throughput microscopy is required. Such applications include imaging and detection of bioparticles of interest in oceanography (e.g., phytoplanktons), energy science (e.g., oil emulsions and engineered microbes), environmental science, food science, cosmetics, pharmaceutics, and medicine (e.g., other rare cell types listed in Table S4).

Materials and Methods

The initial concentration of cells that were used for the rare cell detection measurements was determined by a hemacytometer. Four counts were performed and the mean and standard deviation were calculated. Clusters of

cells were counted as a single cell. The fate of these clusters in the microfluidic device is unclear; clusters could be filtered out upstream, traverse the channel as a cluster, or break up into smaller clusters or individual cells. The coated MCF7 cells were diluted into 3 mL of lysed blood. The resulting concentrations were 0, 5, 10, 50, 100, and 500 coated MCF7 cells per 3 mL. The standard deviation of the initial count is expected to decrease by the dilution factor for each spiked sample. Other sources of error, such as in the process of pipetting, are more difficult to quantify due to the lack of comparable technology for detecting extremely rare events or low concentrations of cells. The fit function used in Fig. 4*C* is $y = ax + b$, where x and y are the spiked and captured numbers of MCF7 cells, respectively, a is the capture efficiency, and b is the contamination. For large x, the fit function asymptotically approaches $y = ax$. From the fit, the capture efficiency was found to be 75% with a coefficient of determination of 0.94, indicating that the regression line represents the data well.

ACKNOWLEDGMENTS. We thank T. Fukuhara for valuable discussions, Y. Liu for assistance with the experiments, and L. Vandenberghe for his suggestion to use the SVM. We acknowledge support from the U.S. Congressionally Directed Medical Research Programs (W81XWH1010519), the Microsystems Technology Office in the U.S. Defense Advanced Research Projects Agency, the National Institutes of Health (NIH), and Caltech-UCLA Joint Center for Translational Medicine. K. G. holds a Career Award at the Scientific Interface from the Burroughs Wellcome Fund. J. A. and C. W. are supported by the German Research Foundation and the Natural Sciences and Engineering Research Council of Canada, respectively. The flow cytometry experiment was performed in the Jonsson Comprehensive Cancer Center (JCCC) and Center for AIDS Research Flow Cytometry Core Facility at the University of California, Los Angeles (UCLA), that is supported by the NIH awards CA-16042 and AI-28697 and by the JCCC, the UCLA AIDS Institute, and the David Geffen School of Medicine at UCLA.

1. Mertz JC (2009) *Introduction to Optical Microscopy* (Roberts and Company Publishers, Greenwood Village, CO).
2. Pawley J (2006) *Handbook of Biological Confocal Microscopy* (Springer, New York).
3. Drapcho C, Nghiem J, Walker T (2008) *Biofuels Engineering Process Technology* (McGraw-Hill Professional, New York).
4. Wollman R, Stuurman N (2007) High throughput microscopy: From raw images to discoveries. *J Cell Sci* 120:3715–3722.
5. Tse HTK, Meng P, Gossett DR, Irturk A, Kastner R, Di Carlo D (2011) Strategies for implementing hardware-assisted high-throughput cellular image analysis. *J Lab Autom* 16:422–430.
6. Ash EA, Nicholls G (1972) Super-resolution aperture scanning microscope. *Nature* 237:510–512.
7. Chi KR (2009) Super-resolution microscopy: Breaking the limits. *Nat Methods* 6:15–18.
8. Hell SW (2007) Far-field optical nanoscopy. *Science* 316:1153–1158.
9. Conrad C, Gerlich DW (2010) Automated microscopy for high-content RNAi screening. *J Cell Biol* 188:453–461.
10. Lang P, Yeow K, Nichols A, Scheer A (2006) Cellular imaging in drug discovery. *Nat Rev Drug Discov* 5:343–356.
11. Basiji DA, Ortyn WE, Liang L, Venkatachalam V, Morrissey P (2007) Cellular image analysis and imaging by flow cytometry. *Clin Lab Med* 27:653–670.
12. Brown L (2011) Characterizing biologics using dynamic imaging particle analysis. *BioPharm Int* 24:s2–s7.
13. Coulter WH (1953) Means for counting particles suspended in a fluid. US Patent 2656508.
14. Zhe J, Jagtiani A, Dutta P, Hu H, Carletta J (2007) A micromachined high throughput Coulter counter for bioparticle detection and counting. *J Micromech Microeng* 17:304–313.
15. Shapiro HM (2003) *Practical Flow Cytometry* (Wiley-Liss, New York).
16. Bonner WA, Hulett HR, Sweet RG, Herzenberg LA (1972) Fluorescence activated cell sorting. *Rev Sci Instrum* 43:404–409.
17. Nishino N, et al. (2005) High-speed 2-D image measurement for plasma-wall interaction studies. *J Nucl Mater* 337:1073–1076.
18. Tiwari V, Sutton MA, McNeill SR (2007) Assessment of high speed imaging systems for 2D and 3D deformation measurements: Methodology development and validation. *Exp Mech* 47:561–579.
19. Thoroddsen ST, Etoh TG, Takehara K (2008) High-speed imaging of drops and bubbles. *Annu Rev Fluid Mech* 40:257–285.
20. Holst GC, Lomheim TS (2011) *CMOS/CCD Sensors and Camera Systems* (SPIE Publications, Bellingham).
21. Baker M (2011) Faster frames, clearer pictures. *Nat Methods* 8:1005–1009.
22. Goda K, Tsia KK, Jalali B (2009) Serial time-encoded amplified imaging for real-time observation of fast dynamic phenomena. *Nature* 458:1145–1149.
23. Goda K, Tsia KK, Jalali B (2008) Amplified dispersive Fourier-transform imaging for ultrafast displacement sensing and barcode reading. *Appl Phys Lett* 93:131109.
24. Di Carlo D (2009) Inertial microfluidics. *Lab Chip* 9:3038–3046.
25. Di Carlo D, Irimia D, Tompkins RG, Toner M (2007) Continuous inertial focusing, ordering, and separation of particles in microchannels. *Proc Natl Acad Sci USA* 104:18892–18897.
26. Gossett DR, Di Carlo D (2009) Particle focusing mechanisms in curving confined flows. *Anal Chem* 81:8459–8465.
27. Lee W, Amini H, Stone HA, Di Carlo D (2010) Dynamic self-assembly and control of microfluidic particle crystals. *Proc Natl Acad Sci USA* 107:22413–22418.
28. Sollier E, Murray C, Maoddi P, Di Carlo D (2011) Rapid prototyping polymers for microfluidic devices and high pressure injections. *Lab Chip* 11:3752–3765.
29. Goda K, Solli DR, Tsia KK, Jalali B (2009) Theory of amplified dispersive Fourier transformation. *Phys Rev A* 80:043821.
30. Goda K, Jalali B (2010) Noise figure of amplified dispersive Fourier transformation. *Phys Rev A* 82:033827.
31. Chou J, Boyraz O, Solli DR, Jalali B (2007) Femtosecond real-time single-shot digitizer. *Appl Phys Lett* 91:161105.
32. Solli DR, Chou J, Jalali B (2008) Amplified wavelength-time transformation for real-time spectroscopy. *Nat Photonics* 2:48–51.
33. Kilts S (2007) *Advanced FPGA Design: Architecture, Implementation, and Optimization* (Wiley-IEEE Press, New York).
34. Sawww R, Schmidt AG (2010) *Embedded Systems Design with Platform FPGAs: Principles and Practices* (Morgan Kaufmann, New York).
35. Cristianini N, Shawe-Taylor J (2000) *An Introduction to Support Vector Machines and Other Kernel-Based Learning Methods* (Cambridge University Press, Cambridge, UK).
36. Wang L (2005) *Support Vector Machines: Theory and Applications* (Springer, New York).
37. Huls PG, et al. (1992) A computer-aided measuring system for the characterization of yeast populations combining 2D-image analysis, electronic particle counter, and flow cytometry. *Biotechnol Bioeng* 39:343–350.
38. Calvert ME, Lannigan JA, Pemberton LF (2008) Optimization of yeast cell cycle analysis and morphological characterization by multispectral imaging flow cytometry. *Cytometry A* 73:825–833.
39. Little MT, Storb R (2002) History of hematopoietic stem-cell transplantation. *Nat Rev Cancer* 2:231–238.
40. Moon JJ, et al. (2009) Tracking epitope-specific T cells. *Nat Protoc* 4:565–581.
41. Cristofanilli M, et al. (2004) Circulating tumor cells, disease progression, and survival in metastatic breast cancer. *N Engl J Med* 351:781–791.
42. Nagrath S, et al. (2007) Isolation of rare circulating tumor cells in cancer patients by microchip technology. *Nature* 450:1235–1239.
43. Rosenblatt JI, Hokanson JA, Mclaughlin SR, Leary JF (1997) Theoretical basis for sampling statistics useful for detecting and isolating rare cells using flow cytometry and cell sorting. *Cytometry* 27:233–238.
44. Zweig MH, Campbell G (1993) Receiver-operating characteristic (ROC) plots: A fundamental evaluation tool in clinical medicine. *Clin Chem* 39:561–577.
45. Pepe MS (2004) *The Statistical Evaluation of Medical Tests for Classification and Prediction* (Oxford University Press, New York).